New Journal of Physics
The open access journal at the forefront of physics

Deutsche Physikalische Gesellschaft DPG
IOP Institute of Physics

Published in partnership with: Deutsche Physikalische Gesellschaft and the Institute of Physics

OPEN ACCESS

RECEIVED
15 August 2015

ACCEPTED FOR PUBLICATION
28 September 2015

PUBLISHED
26 October 2015

PAPER

Thermal gating of charge currents with Coulomb coupled quantum dots

H Thierschmann[1,3], F Arnold[1], M Mittermüller[1], L Maier[1], C Heyn[2], W Hansen[2], H Buhmann[1] and L W Molenkamp[1]

[1] Physikalisches Institut (EP3), Universität Würzburg, Am Hubland, D-97074, Würzburg, Germany
[2] Institut für Nanostruktur- und Festkrperphysik, Universität Hamburg, Jungiusstrasse 11, D-20355 Hamburg, Germany
[3] Present address: Kavli Institut of Nanoscience, Faculty of Applied Sciences, Delft University of Technology, Lorentzweg 1, 2628CJ Delft, The Netherlands.

E-mail: h.r.thierschmann@tudelft.nl **and** laurens.molenkamp@physik.uni-wuerzburg.de

Keywords: quantum dot systems, Coulomb interaction, thermoelectrics, thermal gating, three-terminal device

Abstract

We have observed thermal gating, i.e. electrostatic gating induced by hot electrons. The effect occurs in a device consisting of two capacitively coupled quantum dots. The double dot system is coupled to a hot electron reservoir on one side (QD1), while the conductance of the second dot (QD2) is monitored. When a bias across QD2 is applied we observe a current which is strongly dependent on the temperature of the heat reservoir. This current can be either enhanced or suppressed, depending on the relative energetic alignment of the QD levels. Thus, the system can be used to control a charge current by hot electrons.

1. Introduction

In recent years thermoelectrics, thermionics and thermal management in small-scaled devices have become important subjects both in basic and applied solid-state research [1, 2]. In order to control the heat flow on the nanometer scale, a number of promising concepts have been proposed, and partly realized, including solid-state thermal rectifiers [3–7], thermal transistors [8, 9], and nano-refrigerators [10, 11]. Moreover, new concepts for highly efficient energy harvesting devices have recently been discussed [12, 13] which use a system of two quantum dots (QDs) as a central building block to convert heat into a directed current. The key feature of these systems is the capacitive inter-dot coupling [14] which enables energy exchange between the QDs while particle transfer is blocked. Here we show how a system of two Coulomb coupled QDs acts as a thermal gate for charge currents. One of the dots (QD1) can exchange electrons with a hot reservoir only. The other dot (QD2) connects two reservoirs of equal but lower temperature. If a small potential difference is applied across QD2, we observe that the resulting current can be either enhanced or suppressed by variation of the temperature in the hot bath connected to QD1. An intuitive picture is given which explains the underlying mechanism. It is shown that this effect of thermal gating is in fact strongly related to correlations between fluctuations in the occupation number of both QDs.

2. Experimental setup

The device is processed by means of optical and *e*-beam lithography and subsequent metalization of Ti/Au-electrodes (gates) on a GaAs/AlGaAs heterostructure with a two-dimensional electron gas (2DEG) 94 nm below the surface (carrier density $n = 2.4 \times 10^{11}\,\mathrm{cm}^{-2}$, electron mobility $\mu = 0.69 \times 10^{6}\,\mathrm{cm}^{2}\,\mathrm{V}^{-1}\,\mathrm{s}^{-1}$). The gate structure is shown in figure 1 (a). The gates (black) are labeled 1 through 7, P1 and P2. The electron reservoirs are denoted S, D and H. The QDs are defined by gates 3 to 7, labeled QD1 and QD2. QD1 is in direct contact with reservoir H, which will serve as a hot electron reservoir. QD2 is connected to reservoirs S and D which are at a lower temperature, representing the conductor circuit. The junctions are tuned into the tunneling regime. The

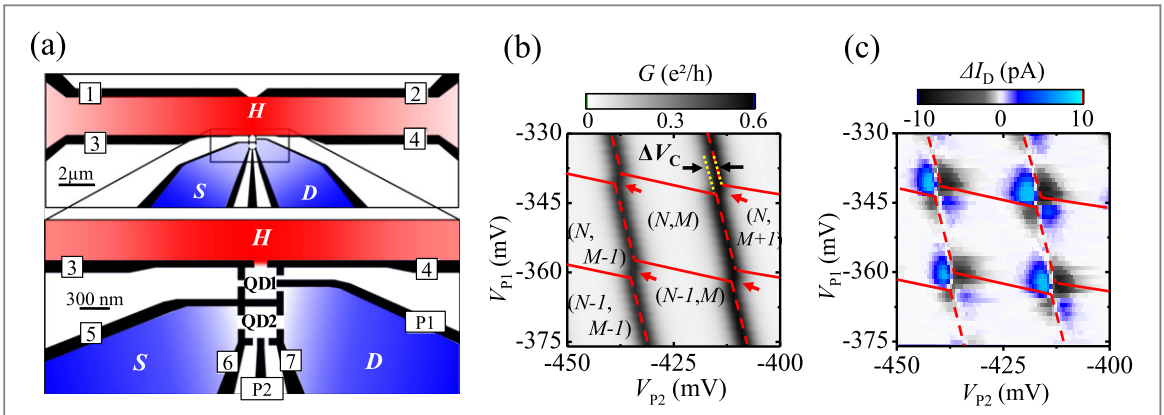

Figure 1. (a) Schematic design of the gate structure (black). Gates are labeled with numbers 1–7, P1 and P2. Electronic reservoirs are denoted S, D (both blue) and H (red). (**b**) Stability diagram of the QD-system showing the conductance of QD2. The characteristic honeycombs are indicated with red lines. QD occupation numbers are denoted with N, M. ΔV_C indicates the capacitive inter-dot coupling energy. (**c**) Current signal ΔI_D in reservoir D with $V_{S,GND} \approx -30\ \mu$V for $T_H \approx T_{S,D} + 100$ mK.

plunger-gate voltages P1 and P2 control the chemical potentials $\mu^{(1)}$ and $\mu^{(2)}$ of the QDs such that the electron occupation numbers can be adjusted individually. The two QDs are separated by an electrostatic barrier (gate 5), which suppresses the electron transfer between the dots. At the same time, QD1 and QD2 interact electrostatically due to the small spatial separation. Hence, the occupation number of each QD affects the chemical potential of the other QD, and thus $\mu^{(1)} = \mu^{(1)}(N, M)(\mu^{(2)} = \mu^{(2)}(N, M))$, where N and M are the occupation numbers of QD1 and QD2, respectively [14, 16]. Reservoir H defined by gates 1, 2, 3 and 4 forms a channel of 20 μm length and 2 μm width. Opposite QD1, a constriction is created by gates 1 and 2 which serves as a voltage probe in the channel. Its conductance is set to $G = 10\ e^2\ h^{-1}$, thus ensuring that no thermovoltage is created across this junction when the temperature in reservoir H is increased [17].

The sample is mounted in a top-loading dilution refrigerator with base temperature $T_{base} = 80$ mK. For a conductance characterization of QD2 with all reservoirs at T_{base}, an excitation voltage $V_{ac} = 5\ \mu$V ($f = 113$ Hz) is applied between reservoirs S and D. The current is measured with a lock-in, using a current amplifier that connects D to a virtual ground potential. By varying V_{P1} and V_{P2} one obtains the so-called stability diagram of the QD-system [16], shown in figure 1 (b) where the conductance G of QD2 is displayed in a gray scale as a function of the voltages V_{P1} and V_{P2}.

Along the horizontal axis V_{P2}, we observe two conductance resonances which identify those gate voltage configurations for which $\mu^{(2)}$ is aligned with μ_S and μ_D. They are separated by the Coulomb charging energy of QD2. Due to the mutual capacitive coupling the energetic position of $\mu^{(2)}$ is affected by the energy of QD1. This leads to a continuous shift of the conductance resonances for larger V_{P1} towards smaller V_{P2} (dashed, red lines in figure 1(b)). When $\mu^{(1)}$ aligns with μ_H, N changes by one (solid, red lines in figure 1(b)). This causes discrete jumps for the conductance resonances of QD2, indicated by red arrows in figure 1 (b). These jumps are a result of the capacitive inter dot coupling which leads to the transfer of the energy E_C: $\mu^{(2)}(N + 1, M) = \mu^{(2)}(N, M) + E_C$ [14, 16]. Hence, the charge occupation numbers of both QD1 and QD2 are stable only in the regions enclosed by solid and dashed lines. The energy E_C can be calculated from the displacement of the conductance resonance along the V_{P2}-direction, ΔV_C, indicated by yellow dotted lines in the figure. Using the gate efficiency $\alpha_2 = 0.032$ obtained from dI/dV characterization of QD2 yields $E_C \approx 90\mu$V.

In order to subject the QD-system to a temperature difference, we make use of the commonly used current heating technique [4, 17–19]: an ac-current I_h is applied to the heating channel (reservoir H) where it heats the electron gas locally due to Joule heating, while the large reservoirs stay at base temperature. Based on QPC-thermometry [17] we estimate that for $I_h = 150$ nA with frequency $f = 113$ Hz, T_H increases by $\Delta T \approx 100$ mK. The ac-heating causes the temperature in the heat reservoir to oscillate at $2f = 226$ Hz between T_{base} and $T_{max} = T_{base} + \Delta T$. This ensures that all temperature-driven effects also oscillate at $2f$, enabling straight forward lock-in detection. In order to rule out unwanted $2f$ contributions resulting from direct capacitive coupling between the heating channel and the QD system, we fix the electro-chemical potential at the center of the channel by grounding the reservoir behind the QPC formed by gates 1 and 2. This ensures that the ac-heating voltage oscillates symmetrically with respect to this point. Next, a dc-voltage source is connected to S ($V_{S,GND}$) while a current amplifier connecting D to ground is used to monitor the current signal at $2f$. This allows us to determine the change of the current in the drain contact ΔI_D due to variation of T_H.

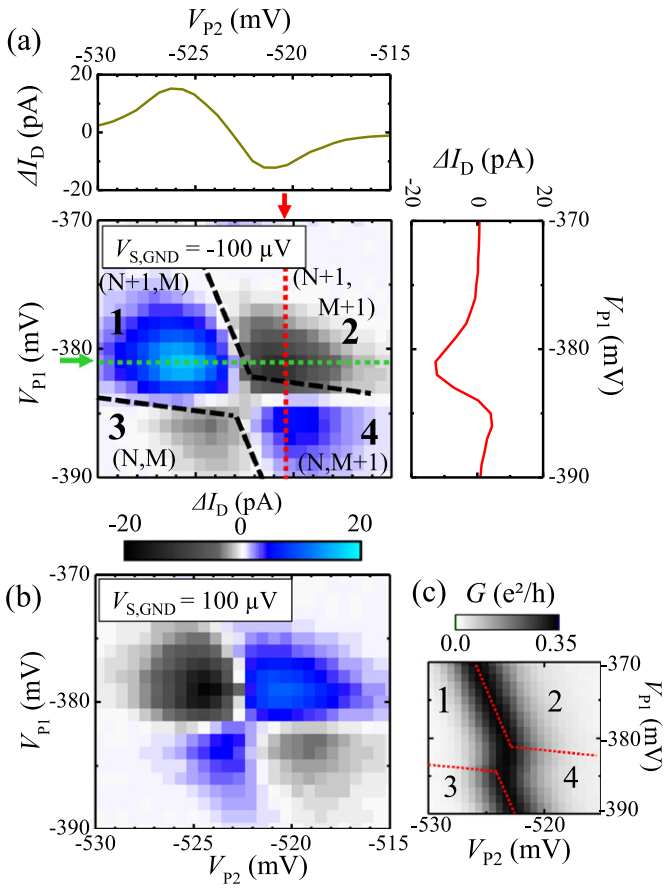

Figure 2. (a) Color scale plot of the change of current ΔI_D with T_H in the region of the honeycomb vertex. Black, dashed lines indicate the boundaries of the stability regions denoted 1–4. Data taken for $V_{S,GND} = -100\ \mu V$. Top and side panel show single traces extracted for $V_{P1} = -381$ mV and $V_{P2} = -521$ mV, indicated by horizontal (green) and vertical (red) line in the color scale plot (**b**) Data taken for inverted bias voltage: $V_{S,GND} = 100\ \mu V$. (**c**) Conductance stability diagram for the same gate voltage region.

3. Results

With $V_{S,GND} \approx -30\ \mu V$ we obtain the data shown in figure 1(c). The lines delimiting the stability regions are indicated. Surrounding each stability region vertex we observe a four-leaf clover shaped structure that is composed of positive and negative current changes of up to $\pm$ 8 pA. The sign changes occur at the transitions from one quarter of a 'clover leave' to the adjacent ones. Diagonally opposite regions exhibit identical sign. A closeup of a similar clover-leaf structure is given in figure 2 (a) for slightly different values of V_{P1} and V_{P2}, and for $V_{S,GND} = -100\ \mu V$. (For the measurements shown in figure 2 the current amplifier is replaced by a resistor $R = 100\ k\Omega$, the voltage drop across which is detected by the lock-in at $2f$.) The corresponding conductance stability vertex is shown in figure 2(c). A direct comparison identifies the four parts of the clover-leaf pattern with different stability regions of the vertex: sections 1 $(N+1, M)$ and 4 $(N, M+1)$ produce a positive signal while for sections 2 $(N+1, M+1)$ and 3 (N, M) negative ΔI_D are observed. A single trace extracted from the color scale plot for constant $V_{P1} = -381$ mV (green, horizontal line) is shown in the top panel of figure 2 (a). It exhibits a maximum and a minimum at V_{PG} corresponding to dot occupation $(N+1, M)$ and $(N+1, M+1)$, respectively. In between, the signal changes approximately linearly with V_{P2}. Moving further away from the vertex causes the signal to decay. A trace extracted along the V_{P1} axis for constant $V_{P2} = -521$ mV (red, vertical line) behaves likewise (side panel). In a next step the dc-voltage applied to S is reversed, so that $V_{S,GND} = 100\mu V$. The result is given in figure 2 (b). Clearly, the clover leaf pattern is reproduced, however, with all signs inverted.

We now discuss qualitatively how we can understand this behavior. As it is evident from figure 2, the sign of ΔI_D does not change over a single stability section of the system (labeled 1–4 in figures 2 (a) and (c)). Furthermore, the $2f$-detection of the signal indicates that these current signals are related to a temperature change in reservoir H. In the vertex region, the occupation numbers of both QDs can fluctuate while the occupation number becomes fixed when moving away from this region. It is thus apparent that the current changes which give rise to the clover-leaf structure originate from fluctuating occupation numbers of QD1 and

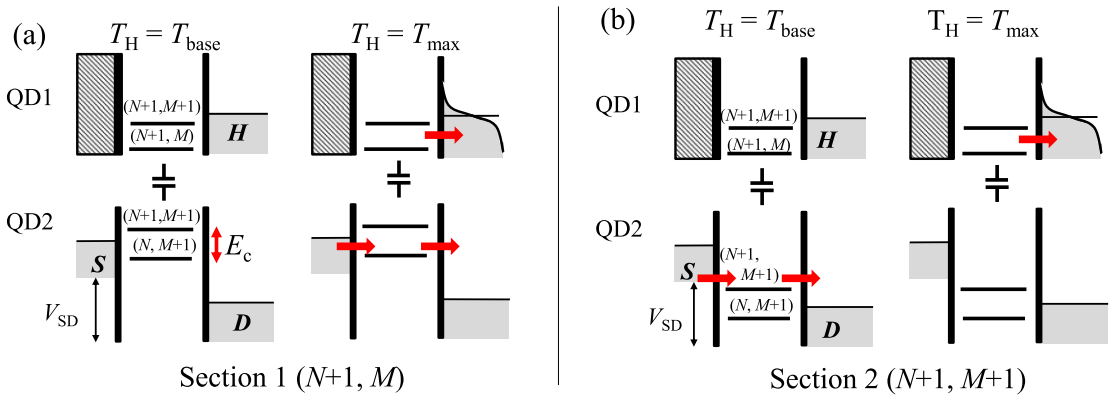

Figure 3. Schematic energy diagram of the QD-system showing the alignment of chemical potentials for stability regions (**a**) $(N+1,\ M)$, section 1 and (**b**) $(N+1,\ M+1)$, section 2. Each configuration is shown for low temperature (left) and high temperature (right) in reservoir H and with finite V_{SD}. Red arrows indicate enhanced occupation fluctuations.

QD2. As an example, figure 3(a) shows the alignment of $\mu^{(1)}$ and $\mu^{(2)}$ for $V_{SD} < 0$ in section 1 (figure 2 (a)). This section corresponds to the region of the stability diagram where QD1 is occupied with $N+1$ electrons and QD2 with M electrons. Due to the ac-character of the heating current the temperature of the heated reservoir T_H oscillates between the two values $T_H = T_{base}$ and $T_H = T_{max} > T_{base}$. For $T_H = T_{base}$ (figure 3 (a), left panel) transport across QD2 is blocked: because the electron number on QD1 is fixed, $\mu^{(1)} < \mu_H$ for both charge configuration of QD2, and the only possible transport channel $\mu^{(2)}(N+1, M+1)$ is outside the bias window of V_{SD}. The situation changes for $T_H = T_{max}$. The elevated temperature now allows the electron number on QD1 to fluctuate (figure 3 (a), right panel). Hence, the energy required to add an electron to QD2 is reduced by E_C whenever QD1 relaxes to the N-state. This makes the $\mu^{(2)}(N, M+1)$ state available for transport. For an increased T_H the rate of fluctuations on QD1 increases and thus the probability of the $\mu^{(2)}(N,\ M\ +\ 1)$ level to open for transport. Temperature and current modulation are in phase and the lock-in amplifier will give a positive current signal.

The corresponding QD levels for section 2 (figure 2 (a)) are depicted in figure 3 (b). The QD occupation is $(N+1, M+1)$. Starting the considerations again for $T_H = T_{base}$ (figure 3(b), left panel) one finds that the occupation number of QD1 is again fixed. However, now $\mu^{(2)}(N+1, M+1)$ is within the bias window V_{SD} and transport across QD2 is enabled. With T_H approaching T_{max} charge fluctuations on QD1 increase. Thus, the probability for the $\mu^{(2)}(N, M+1)$ state increases which blocks transport and reduces the current across QD2. An increasing temperature now results in a decreased current signal. The detected signal appears negative. The sign of current signal in sections 3 and 4 can be explained in an analogous way. The only difference is that QD1 is in the N electron state and fluctuations lead to an occasional occupation of the $N+1$ electron state, which lead to a reversal of the situation described for sections 1 and 2. The overall sign change under reversed voltage bias condition (see figures 2 (a) and (b)) becomes also explainable: because a sign change of the bias voltage reverses the dc-current through QD2 this leads to an overall reversal of the observed signal.

We would like to note that a similar four-leafed clover pattern has been observed in connection with Coulomb coupled double QDs previously by McClure *et al* [15] in a shot noise experiment. The underlying mechanism is actually closely related to our experiments: negatively correlated shot noise indicates that charge fluctuations of one QD tend to suppress fluctuations on the other one (and vice versa). Correspondingly, those are the configurations where we observe a reduced current through QD2 for increasing temperature. Similarly, positive shot noise correlations correspond to a situation where we observe an enhanced current with temperature.

4. Model calculation

We have performed simple model calculations to substantiate the qualitative discussion presented above. Assuming sequential transport across QD2, the current I_D can be related to the applied difference in electrochemical potential $V_{SD} = \mu_S - \mu_D$ by considering Fermi–Dirac occupation statistics $f(\mu^{(2)},\ T_j) = 1/(1 + \exp(\mu^{(2)} - \mu_j/k_B T_j))$, j=S, D in the source and the drain contact and a single resonant QD level $\mu'^{(2)}$ which is located at $\mu^{(2)} = -E_C/2$. For $\mu_S < \mu_D$ we can then write

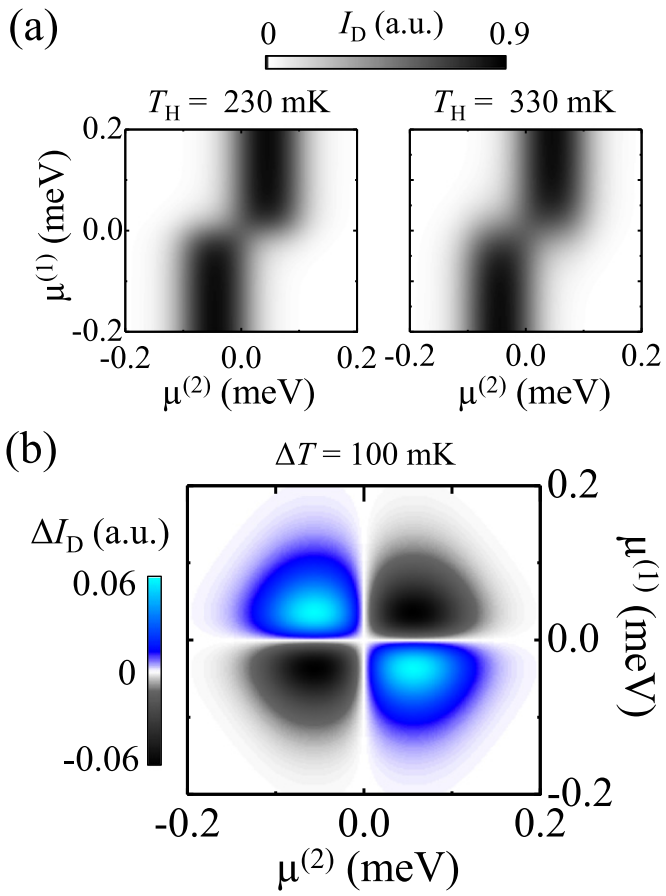

Figure 4. Model calculations for I_D and ΔI_D. The following parameters were used: $T_{S,D} = T_{base} = 230$ mK, $\mu_S = -\mu_D = -50$ μeV, $\mu_H = 0$ and $E_C = 90$ μeV. (**a**) I_D for $T_H = 230$ mK (left) and $T_H = 330$ mK (right). (**b**) Subtraction of the figures given in (a) yields $\Delta I_D = I_D(T_H = 330\ \text{mK}) - I_D(T_H = 230\ \text{mK})$.

$$I'_D\left(\mu^{(2)}\right) \propto f\left(-E_C/2,\ T_S\right) \times \left[1 - f\left(-E_C/2,\ T_D\right)\right]. \tag{1}$$

The current I''_D across QD2 when QD1 hosts N+1 electrons can be treated likewise, with $\mu^{(2)} = +E_C/2$. The total current I_D through QD2 is now the sum of I'_D and I''_D, weighted with the appropriate probabilities of QD1 hosting N or $N+1$ electrons. Thus,

$$I_D\left(\mu^{(1)},\ \mu^{(2)}\right) \propto f\left(\mu^{(1)},\ T_H\right) I'_D + \left(1 - f\left(\mu^{(1)},\ T_H\right)\right) I''_D. \tag{2}$$

Figure 4(a) compares I_D as a function of $\mu^{(1)}$ and $\mu^{(2)}$ for $T_H = T_{base}$ (left) and $T_H = T_{base} + \Delta T = T_{max}$ with $\Delta T = 100$ mK (right) while $T_{S,D} = T_{base} = 230$ mK, $\Delta\mu = 100$ μV and $E_C = 90$ μV. As expected, the results strongly resemble the conductance stability diagram in the vertex region. However, major differences for different T_H are not directly obvious. In order to model the current change through QD2 we calculated $\Delta I_D = I_D(T_{max}) - I_D(T_{base})$, which corresponds to the change in current through QD2 due to a change of T_H by ΔT. The result reproduces nicely the clover-leaf pattern (figure 4(b)).

5. Discussion

We point out that a similar device geometry can be used to create a QD heat engine [12, 13]. However, in contrast to the experiments presented here, the performance of such a heat engine directly depends on the asymmetry of tunneling rates of QD2 to reservoirs S and D. Additionally, an applied bias voltage between S and D constitutes a high load which strongly suppresses the heat conversion process [12]. Therefore, no signature of a QD heat engine is expected to be observable in the present experiments. The effect we have observed in a Coulomb coupled double QD is that a driven charge current through one dot can be gated by changing the electron temperature of the reservoir which is connected the second dot. This effect can not only be used, e.g., to monitor carrier heating in quantum circuits but also it enables the direct manipulation of a current in a non-local manner by varying the temperature of a remote electron reservoir. We can estimate the gating range of our device by

analyzing the data shown in figures 2(a) and (c): Using the G of QD2 at those configurations for which a maximal $\Delta I_D = 18$ pA is observed ($G = 0.09\ e^2\ h^{-1}$) we calculate the drain current for $V_{S,GND} = -100\,\mu$V and $T_H = T_{base}$, which gives $I_D = 360$ pA. Relating this current to ΔI_D then yields a gating amplitude of 5%. Although this ratio is rather small, it can be strongly enhanced by tuning the parameters E_C and $k_B \Delta T$.

Furthermore, thermal gating could be utilized to also manipulate heat flow across QD2: since the thermal conductance κ of a QD as a function of μ usually follows the Wiedemann–Franz rule and thus has a similar line shape as the conductance [20], the mechanism presented here would allow gating of heat currents to be accomplished, thus suggesting a route to realizing a QD-based all thermal transistor.

6. Conclusion

In this paper we have explored the effect of thermal gating, i.e., the possibility to use the temperature in a hot electron reservoir connected to a QD to manipulate and to control the charge current through a second, electrostatically coupled QD at a lower temperature. The effect is most efficient in the vertex regime of the stability diagram. Depending on the energy level alignment chosen for the individual QDs, thermal gating leads to either an enhancement or a suppression of the charge current. The resulting characteristic 'clover leaf' pattern is successfully explained within a picture of thermal fluctuation introduced to the hot QD and it is qualitatively reproduced with model calculations. Our results suggest that with this three-terminal design also the realization of pure thermal transistors becomes feasible.

Acknowledgments

The authors gratefully acknowledge discussions with B Sothmann, R Sánchez and M Büttiker. This work has been financially supported by the Deutsche Forschungsgemeinschaft (SPP1386).

References

[1] Giazotto F, Heikkilä T T, Luukanen A, Savin A M and Pekola J P 2006 *Rev. Mod. Phys.* **78** 217
[2] Shakouri A 2011 *Annu. Rev. Mater. Res.* **41** 399
[3] Terraneo M, Peyrad M and Casati G 2002 *Phys. Rev. Lett.* **88** 094302
[4] Scheibner R, König M, Reuter D, Wieck A D, Gould C, Buhmann H and Molenkamp L W 2008 *New J. Phys.* **10** 083016
[5] Matthews J, Sánchez D, Larsson M and Linke H 2012 *Phys. Rev.* B **85** 205309
[6] Tseng Y-C, Kuo D M T, Chang Y-C and Lin Y-T 2013 *Appl. Phys. Lett.* **103** 053108
[7] Chang C W, Okawa D, Majumdar A and Zettl A 2006 *Science* **314** 1121
[8] Yigen S and Champagne A 2014 *Nano Lett.* **14** 289
[9] Ben-Abdallah P and Biehs S-A 2014 *Phys. Rev. Lett.* **112** 044301
[10] Whitney R S 2013 *Phys. Rev.* B **88** 064302
[11] Prance J R, Smith C G, Griffiths J P, Chorley S J, Anderson D, Jones G A C, Farrer I and Ritchie D A 2009 *Phys. Rev. Lett.* **102** 146602
[12] Sánchez R and Büttiker M 2011 *Phys. Rev.* B **83** 085428
[13] Thierschmann H, Sánchez R, Sothmann B, Arnold F, Heyn C, Hansen W, Buhmann H and Molenkamp L W 2015 *Nat. Nanotechnology* **10** 854
[14] Molenkamp L W, Flensberg K and Kemerink M 1995 *Phys Rev. Lett.* **75** 4282
[15] McClure D T, DiCarlo L, Zhang Y, Engel H-A, Marcus C M, Hanson M P and Gossard A C 2007 *Phys. Rev. Lett.* **98** 056801
[16] van der Wiel W G, De Franceschi S, Elzerman J M, Fujisawa T, Tarucha S and Kouwenhoven L P 2002 *Rev. Mod. Phys.* **75** 1
[17] Molenkamp L W, van Houten H, Beenakker C W J, Eppenga R and Foxon C T 1990 *Phys. Rev. Lett.* **65** 1052
[18] Staring A A M, Molenkamp L W, Alphenaar B W, van Houten H, Buyk O J A, Mabesoone M A A, Beenakker C W J and Foxon C T 1993 *Europhys. Lett.* **22** 57
[19] Thierschmann H, Henke M, Knorr J, Maier L, Heyn C, Hansen W, Buhmann H and Molenkamp L W 2013 *New J. Phys.* **15** 123010
[20] Guttman G D, Ben-Jacob E and Bergman D J 1995 *Phys. Rev.* B **51** 17758